Motion of a Viscoelastic Micellar Fluid around a Cylinder: Flow and Fracture

Joseph R. Gladden* and Andrew Belmonte†

The W. G. Pritchard Laboratories, Department of Mathematics, Pennsylvania State University, University Park, Pennsylvania 16802, USA

(Received 18 May 2006; revised manuscript received 28 February 2007; published 29 May 2007)

We present an experimental study of the motion of a viscoelastic micellar fluid around a moving cylinder, which ranges from fluidlike flow to solidlike tearing and fracture, depending on the cylinder radius and velocity. The observation of crack propagation driven by the cylinder indicates an extremely low tear strength, approximately equal to the steady state surface tension of the fluid. At the highest speeds a driven crack is observed in front of the cylinder, propagating with a fluctuating speed equal on average to the cylinder speed, here as low as 5% of the elastic wave speed.

DOI: 10.1103/PhysRevLett.98.224501 PACS numbers: 47.20.Gv, 46.50.+a, 47.57.−s

By definition, the primary difference between a solid and a fluid is that the former resists an applied force by undergoing a finite deformation while the latter flows, or deforms, continually. Viscoelastic materials combine these aspects in their linear response, either as a viscous, lossy solid or as an elastic fluid [1]. A solid will fail under a large enough force via different mechanisms such as crack formation and propagation (fracture) [2–4]. When viscoelastic materials fail, relaxation processes play a more prominent role, and the dynamics of the failure mechanisms are altered [5–8]. Studying fracture in soft materials holds the benefit of much lower sound speeds, which leads to slower and more accessible crack dynamics [9,10]. Here we focus on the transition to solidlike failure in a concentrated viscoelastic micellar fluid: how do different failure modes arise from the fluidlike dynamics at slower time scales and lower forces?

Viscoelastic micellar fluids are comprised of self-assembling surfactant aggregates and are interesting as soft materials due to the substitution of hydrophobic ''bonds'' for covalent ones in their material properties, a similarity they share with biological membranes [11]. At high concentrations these fluids can be gel-like, although they still flow under small stress, due to the presence of micellar junctions instead of the chemical cross-links of a polymer gel [12,13]. There are a variety of morphologies of these surfactant systems, including onion phases [14], myelins [15], and wormlike micellar fluids; the latter are known for novel rheological behavior [1,16–18] and hydrodynamic instabilities [17,19], but to our knowledge there has been no study of crack propagation. However in a recent experiment on sphere impact into a micellar fluid, a transition from smooth to fractured cavity surface was observed [20], which motivated this study.

In this Letter we present an experiment in which a cylinder is pulled through a shallow layer of viscoelastic micellar fluid, passing from the flowing response of a fluid to the tearing of a solid as the speed of the cylinder is increased. At the highest speeds we observe an unsteady leading crack ahead of the cylinder followed by a ripped-up wake (Fig. 1). In contrast to a cross-linked polymer gel, this material is ''self-healing,'' and the torn surface returns to a smooth, flat state after a few hours. Similar transitions from smooth shapes to driven crack propagation were observed in Saffman-Taylor fingering of associating polymer fluids [21] and colloidal pastes [22].

The concentrated micellar solution we study is well known as a wormlike micellar fluid at lower concentrations: an aqueous solution of the surfactant cetyltrimethylammonium bromide (CTAB) and the organic salt sodium salicylate (NaSal) [1,11,17]. We use 200 mM CTAB and 120 mM NaSal, a system which exhibits both fluid and solidlike behaviors [23]. The CTAB and NaSal (obtained from Aldrich) are dissolved in filtered deionized water without further purification. Each solution is mixed separately at a temperature of ~70 °C [19], then combined and mixed for several hours. The fluid thickens to a gel-like state as it cools, but is poured into the experimental channel or rheometer while still warm (~55 °C); it sits for at least 24 hours before use.

The rheology was measured at a fixed temperature of 22.8 °C with an RFS-III strain rate controlled couette cell rheometer (Rheometric Scientific, now TA Instruments). At low shear rates the flow is Newtonian, with a zero shear viscosity of $\eta_0 \simeq 1670$ P. At higher shear rates the fluid shear thins, and the stress reaches a roughly constant plateau, as is often seen in wormlike micellar fluids

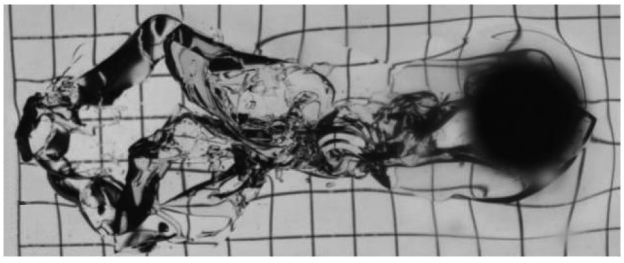

FIG. 1. The initial result of quickly accelerating a cylinder from rest in a concentrated micellar fluid ($d = 9.5$ mm, $U_0 = 77$ mm/s).

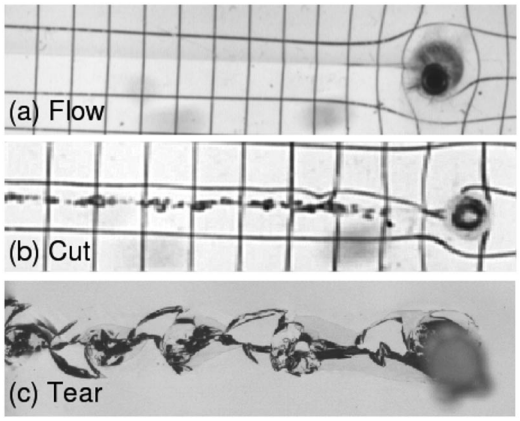

FIG. 2. Responses of a micellar fluid (200/120 mM CTAB/NaSal, depth 2.0 cm) to a cylinder moving at speeds: (a) 2.8 mm/s, $d = 3.1$ mm; (b) 9.9 mm/s, $d = 1.8$ mm; (c) 16 mm/s, $d = 7.9$ mm. The view shown is along the cylinder axis.

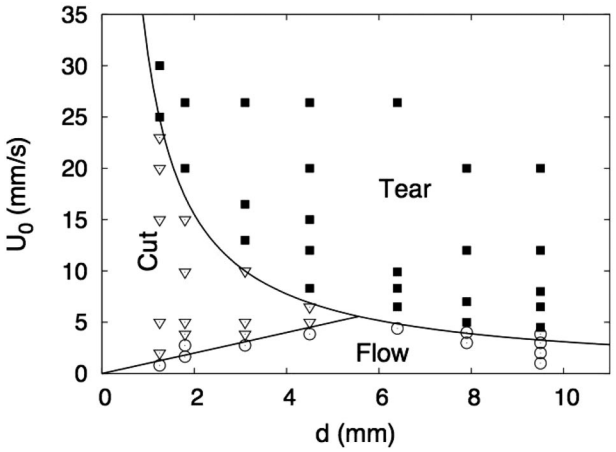

FIG. 3. The phase diagram for a moving cylinder (speed U_0, diameter d) in a micellar fluid layer (depth 2.0 cm). The boundaries represent simple scaling relations (see text).

[1,17]. Dynamic rheology experiments were also performed and found to be well fitted by a Maxwell model for strain frequencies less than about 10 s^{-1}, yielding an elastic shear modulus of $G_0 \simeq 190$ Pa [23]. Both measurements indicated a relaxation time $\lambda \simeq 1.1$ s. The measured density was $\rho \simeq 1.1$ g/cc [23].

We have constructed a linear motion system which pulls a rigid rod (circular or square cross section) through the fluid at speed U_0; our setup was inspired by the Mylar sheet cutting experiments of Roman and co-workers [24]. An acrylic box of dimensions $61 \times 15 \times 5$ cm is filled with warm (pourable) micellar fluid to a depth $H = 0.9$–2.0 cm. The box is mounted on a translation stage driven by a voltage controlled servo motor and ball screw, which maintains a fixed speed $U_0 \simeq 0$–80 mm/s over a range of 83 cm. The rod (size d) is inserted into the fluid, $\sim$0.5 mm from the bottom. Images are captured with a Phantom v5.0 high speed digital video or a Nikon D70 digital SLR camera; the rod and camera are at rest in the lab frame. The experiments were performed at room temperature (22.5–24.5 °C). The flow is very elastic (Deborah number $\mathrm{De} = \lambda U_0/d \simeq 0.5$–$11.5$) while remaining very viscous (Reynolds numbers $\mathrm{Re} = \rho d U_0/\eta_0 \simeq 5 \times 10^{-4}$).

We observe three distinct dynamic responses depending on the size d and speed U_0 of the cylinder, as illustrated in Fig. 2. In the *flow* state, the material smoothly moves around the cylinder and recombines behind it leaving a creased wake, but no trapped air bubbles. At higher speeds, a smooth cavity appears just behind the cylinder, a phenomenon also seen in viscous Newtonian fluids [23]; the material still flows smoothly. In the *cut* state, the material still appears to flow around the cylinder, but the walls of the cavity are textured. This results in air bubbles trapped as the walls recombine [Fig. 2(b)]. In contrast, the *tear* state is characterized by lateral splitting of the cavity walls, resulting in large tears with a characteristic fin shape (Fig. 2). In Fig. 3 we show the material response for various cylinder velocities and diameters ($H = 2.0$ cm). For a large enough cylinder, the transition is directly from flow to tear.

The tearing shape (left panel of Fig. 4) occurs because the crack propagates initially perpendicular to the cavity surface, but curves back as the cylinder advances and the tear opens. A similar effect is responsible for the shape observed when a moving cylinder tears through a thin plastic sheet [24,25]. The curves comprising this shape are well fit by cubic arcs $x - x_0 = Ay^3$ (right panel of Fig. 4), where x_0 is the position directly behind the cylinder, rather than cycloidal arcs [25] or parabolic arcs [26]. For the back (left) side of the tear, the fit parameter $A = 0.011$ mm^{-2} is close to the inverse of the square of the cylinder diameter ($d = 9.5$ mm); this will be investigated in future work.

The transition boundary between flow and cut follows a linear scaling $U_0 \sim d$, equivalent to the critical condition $\mathrm{De} = \mathrm{De}_c$. Thus the onset of texturing occurs when the material does not have time to relax, i.e., when the flow time scale d/U_0 is faster than the relaxation time λ. From the straight line in Fig. 3 we obtain $\mathrm{De}_c \simeq 1.1$. The second transition occurs when the velocity of the cylinder is further increased, either from the cutting state, or at larger diameters directly from the flow state (Fig. 3). The higher velocity tearing state is characterized by lateral cracks in

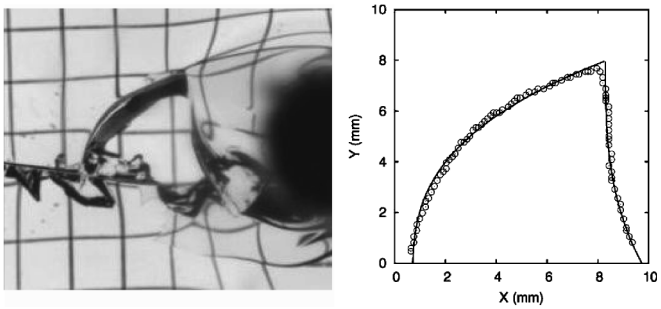

FIG. 4. Detail of the tearing shape, for a $d = 9.5$ mm acrylic cylinder, $U_0 = 77$ mm/s, with two fitted cubic arcs (see text).

the sidewalls of the wake [see Figs. 2(b) and 4]. The transition boundary for tearing seems to be hyperbolic ($U_0 d \sim$ const), with a fitted constant of 31 ± 4 mm^2/s, as shown in Fig. 3.

The tearing regime involves the limited propagation of an apparent crack into the sidewalls of the cavity behind the cylinder. In principle, the scaling of the transition boundary should be obtainable by extending the classic analysis [3] to the viscoelastic case. However, the theory of cracks in highly viscoelastic materials is far from complete [27], and there are many ways to extend the elastic case using various viscoelastic models (see, e.g., [28]). Here we provide a simple scaling argument which reproduces our observations. A surface will rupture when a tangentially directed line force F_l exceeds a critical value $\Gamma_{\rm crit}$, sometimes referred to as the tear strength [3,10] (we will assume that this is a constant for our system). In our experiment the cylinder speed U_0 is fixed, so we obtain an effective force using the approach of Saint-Venant [29,30]: we treat the resistance to the moving cylinder as that of an elastic solid exerting a force $F \sim EAU_0/c$, where E is Young's modulus, $A = Hd$ is the projected cross-sectional area in the direction of motion, and $c = \sqrt{E/\rho}$ is the longitudinal wave speed [29]. The condition for surface rupture (tearing) then occurs for a cylinder such that F exceeds $\Gamma_{\rm crit} H$, or

$$\frac{EU_0 d}{c} > \Gamma_{\rm crit}. \qquad (1)$$

This leads to the hyperbolic boundary shown in Fig. 3.

Combining the measured phase diagram with Eq. (1) allows us to estimate the tear strength of our micellar material. We obtain the Young's modulus from our rheology: $E = 3G_0 \simeq 570$ Pa (assuming the incompressible Poisson ratio 1/2), thus $\Gamma_{\rm crit} \simeq 25 \pm 3$ mN/m. This is significantly lower than typical tear strengths for elastomer gels (e.g., $\sim$10 N/m [10,31]), although it is close to some measured values for the surface free energy of soft materials like polydimethylsiloxane [32]. It is also not far from typical equilibrium surface tensions measured for wormlike micellar fluids: 30–36 mN/m [20,33]. Theoretically, the tear strength can be decomposed into surface energy and dissipative contributions [8,31], and the high tear strength of certain viscoelastic gels is attributed to a high dissipation [8,31]. While it is not unusual for a soft solid to have a surface free energy equal to its surface tension [32] (both defined as the energy required to make new surface area), a measured tear strength so close to the surface tension suggests that dissipation processes are negligible for these slow curving cracks.

At high speeds in the tearing regime, a crack is observed *in front of* the cylinder, see Fig. 5(a). This leading crack is unsteady, swaying side to side, sometimes losing out to another crack. Oscillations in both the transverse (Y) and longitudinal (X) directions [Fig. 5(b)] are like the dynamics of cracks driven in similar experiments using Mylar sheets [24,25]. The tip we observe has a wedge shape with an opening angle $\sim$100° similar to those seen in rubber [34], characteristic of soft materials where a large deformation is needed to achieve the stress levels for propagation [35]. However, these cracks are not driven by remote loading as in Mode I crack propagation [2,3], but by local contact with the moving cylinder. Thus the crack speed follows the cylinder speed U_0; for our material $c \simeq 72$ cm/s, and $U_0/c \simeq 0.05$. A similar slow driven fracture was seen in peeling experiments on gels [10].

Wormlike micellar fluids exhibit a strong flow birefringence so that when viewed through cross polarizers, the stress field can be readily visualized [19,36]. In a birefringent image, monochromatic fringes represent isolines for the stress field, and the spacing is proportional to the stress intensity. For the experiments reported here we find a characteristic dipole pattern around the cylinder, with an asymmetry due to stress relaxation in the wake [23]. The fringes are most closely spaced at the sides of the cylinder, where the shear is maximum; this is also where the cutting instability begins [23]. Surface interactions may also play a role in this transition, analogous to the sharkskin instability in polymer melt extrusion [37].

Cutting is, however, not usually done with a cylinder. We expected a rod with sharper corners—something like a knife—would focus stress at its sharp front edge and cut more directly. Thus we were surprised to find, in a series of similar experiments with a square bar, that high stress began at the *side corners* and formed a detached stress boundary layer which traveled ahead of the square (Fig. 6 for side length $S = 12.5$ mm, $U_0 = 2$ mm/s, De $\simeq 0.18$). The square cut more efficiently in the sense that all instabilities (cut/tear) occurred at higher speeds than the cylinder, much like opening an envelope with a finger leaves ragged edges (tearing) while a letter opener at the same

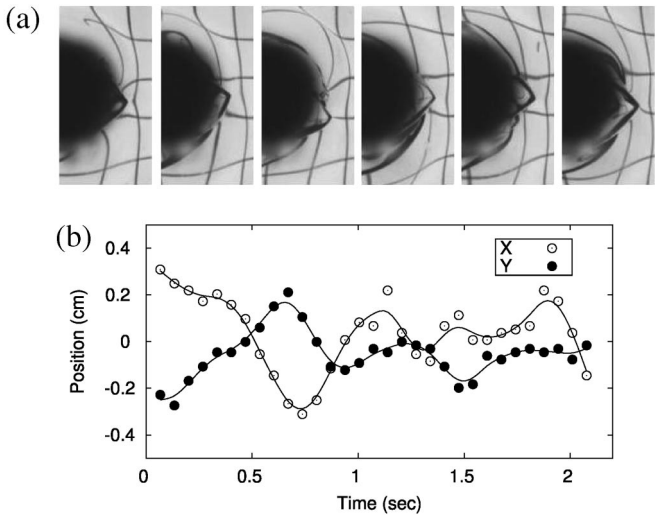

FIG. 5. (a) Oscillating crack preceding the cylinder ($d = 9.5$ mm, $U_0 = 26$ mm/s), with (b) a plot of the horizontal (X) and vertical (Y) positions of the crack tip (origin arbitrary). The solid lines are splines to guide the eye.

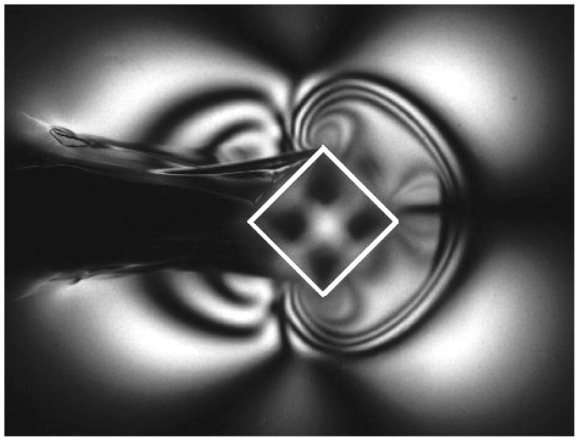

FIG. 6. Birefringent visualization of the micellar fluid layer around a diagonally oriented square "cutting tool" ($S = 12.5$ mm, $U_0 = 2$ mm/s to the right, depth $H = 0.9$ cm). A white outline is superimposed on the outer edge of the square.

speed leaves a cleaner edge [25]. An understanding of these differences remains for a future work.

We have observed transitions from flow to solidlike tearing and fracture in a single material: a concentrated micellar fluid. Comprised of surfactant aggregates weakly held together by the hydrophobic effect [11], this soft material sits at the limit of weak resistance to tear, with a measured tear strength approximately equal to the surface tension. At the highest speeds a crack appears in front of the moving cylinder, propagating with the same speed U_0 unlike a brittle crack driven by remote loading. One could expect a qualitative change in these dynamics as U_0 increases towards some natural speed threshold of the material, perhaps the elastic wave speed. Here we have shown that—from slow crack propagation to tearing and "self-healing"—concentrated micellar materials exemplify the complexity of soft matter systems, demonstrating the variety of dynamics possible in a simple combination of surfactant, salt, and water.

We thank R. H. "Bob" Geist, B. Bitel, and D. Hill for experimental assistance, and E. Sharon, F. Costanzo, G. H. McKinley, A. Mazzucato, and J. Walton for helpful discussions. A. B. acknowledges support from the National Science Foundation (CAREER Grant No. DMR-0094167).

*Present address: Department of Physics and Astronomy, University of Mississippi, Oxford, MS, USA.

†Also at the School of Engineering and Applied Sciences, Harvard University, Cambridge, MA, USA.

[1] R. G. Larson, *The Structure and Rheology of Complex Fluids* (Oxford University Press, New York, 1999).

[2] L. B. Freund, *Dynamic Fracture Mechanics* (Cambridge University Press, Cambridge, England, 1990).

[3] B. Lawn, *Fracture in Brittle Solids* (Cambridge University Press, Cambridge, England, 1993), 2nd ed.

[4] J. A. Hauch, D. Holland, M. P. Marder, and H. L. Swinney, Phys. Rev. Lett. **82**, 3823 (1999).

[5] D. Bonn, H. Kellay, M. Prochnow, K. Ben-Djemiaa, and J. Meunier, Science **280**, 265 (1998).

[6] C. Gay and L. Leibler, Phys. Rev. Lett. **82**, 936 (1999).

[7] C.-Y. Hui, A. Jagota, S. J. Bennison, and J. D. Londono, Proc. R. Soc. A **459**, 1489 (2003).

[8] B. Persson, O. Albohr, G. Heinrich, and H. Ueba, J. Phys. Condens. Matter **17**, R1071 (2005).

[9] A. Livne, G. Cohen, and J. Fineberg, Phys. Rev. Lett. **94**, 224301 (2005).

[10] Y. Tanaka, K. Fukao, and Y. Miyamoto, Eur. Phys. J. E **3**, 395 (2000).

[11] J. Israelachvili, *Intermolecular and Surface Forces* (Academic, New York, 1991), 2nd ed.

[12] M. In, G. Warr, and R. Zana, Phys. Rev. Lett. **83**, 2278 (1999).

[13] T. Koga and F. Tanaka, Eur. Phys. J. E **17**, 225 (2005).

[14] T. Gulik-Krzywicki, J. C. Dedieu, D. Roux, C. Degert, and R. Laversanne, Langmuir **12**, 4668 (1996).

[15] M. Buchanan, S. Egelhaaf, and M. Cates, Langmuir **16**, 3718 (2000).

[16] S. Lerouge, J.-P. Decruppe, and J.-F. Berret, Langmuir **16**, 6464 (2000).

[17] C. Liu and D. Pine, Phys. Rev. Lett. **77**, 2121 (1996).

[18] R. Bandyopadhyay, G. Basappa, and A. K. Sood, Phys. Rev. Lett. **84**, 2022 (2000).

[19] N. Z. Handzy and A. Belmonte, Phys. Rev. Lett. **92**, 124501 (2004).

[20] B. Akers and A. Belmonte, J. Non-Newtonian Fluid Mech. **135**, 97 (2006).

[21] J. Ignés-Mullol, H. Zhao, and J. V. Maher, Phys. Rev. E **51**, 1338 (1995).

[22] E. Lemaire, P. Levitz, G. Daccord, and H. Van Damme, Phys. Rev. Lett. **67**, 2009 (1991).

[23] A. Belmonte and J. R. Gladden (unpublished).

[24] B. Roman, P. Reis, B. Audoly, S. De Villiers, V. Viguié, and D. Vallet, C. R. Mécanique **331**, 811 (2003).

[25] A. Ghatak and L. Mahadevan, Phys. Rev. Lett. **91**, 215507 (2003); **94**, 119901(E) (2005).

[26] B. Audoly, B. Roman, and P. Reis, Phys. Rev. Lett. **94**, 129601 (2005).

[27] See, for instance, the discussion in B. N. J. Persson and E. A. Brener, Phys. Rev. E **71**, 036123 (2005).

[28] Q. S. Nguyen, in *3D Constitutive Relations and Ductile Fracture* (North-Holland, Amsterdam, 1981).

[29] E. A. H. Love, *A Treatise on the Mathematical Theory of Elasticity* (Dover, New York, 1944), 4th ed.

[30] J. R. Gladden, N. Z. Handzy, A. Belmonte, and E. Villermaux, Phys. Rev. Lett. **94**, 035503 (2005).

[31] A. N. Gent, Langmuir **12**, 4492 (1996).

[32] M. Chaudhury, T. Weaver, C. Y. Hui, and E. Kramer, J. Appl. Phys. **80**, 30 (1996).

[33] J. Cooper-White, R. Crooks, and D. Boger, Colloids Surf. A **210**, 105 (2002).

[34] R. Deegan, P. Petersan, M. Marder, and H. Swinney, Phys. Rev. Lett. **88**, 014304 (2001).

[35] M. Marder, Phys. Rev. Lett. **94**, 048001 (2005).

[36] Y. Hu, S. Wang, and A. Jamieson, J. Rheol. (N.Y.) **37**, 531 (1993).

[37] M. M. Denn, Annu. Rev. Fluid Mech. **33**, 265 (2001).